NANO small MICRO

Supporting Information

for *Small,* DOI: 10.1002/smll.202207119

Precision Nanocluster-Based Toroidal and Supertoroidal Frameworks Using Photocycloaddition-Assisted Dynamic Covalent Chemistry

*Kavalloor Murali Lakshmi, Jose V. Rival, Pakath Sreeraj, Sindhu R. Nambiar, Chinnaiah Jeyabharathi, Nonappa, and Edakkattuparambil Sidharth Shibu**

Supporting Information

Precision Nanocluster-Based Toroidal and Supertoroidal Frameworks Using Photocycloaddition-Assisted Dynamic Covalent Chemistry

Kavalloor Murali Lakshmi,[a,b,f] *Jose V. Rival,*[c,f] *Pakath Sreeraj,*[c] *Sindhu R. Nambiar,*[b,d] *C. Jeyabharathi,*[a,b] *Nonappa,*[e] *Edakkattuparambil Sidharth Shibu*[c*]

[a] Council of Scientific and Industrial Research (CSIR)-Central Electrochemical Research Institute (CECRI), Karaikudi-630003, Tamil Nadu, India.

[b] Academy of Scientific and Innovative Research (AcSIR)-CSIR, Ghaziabad-201002, Uttar Pradesh, India.

[c] Smart Materials Lab (SML), Department of Nanoscience and Technology (DNST) University of Calicut (UoC), Malappuram-673635, Kerala, India.

[d] CSIR-Central Food Technological Research Institute (CFTRI), Mysuru-570020, Karnataka, India.

[e] Faculty of Engineering and Natural Sciences, Tampere University, FI-33720, Tampere, Finland.
[f]Equally contributed

*Author for correspondence and reprint requests: shibuchem@gmail.com or shibu@uoc.ac.in

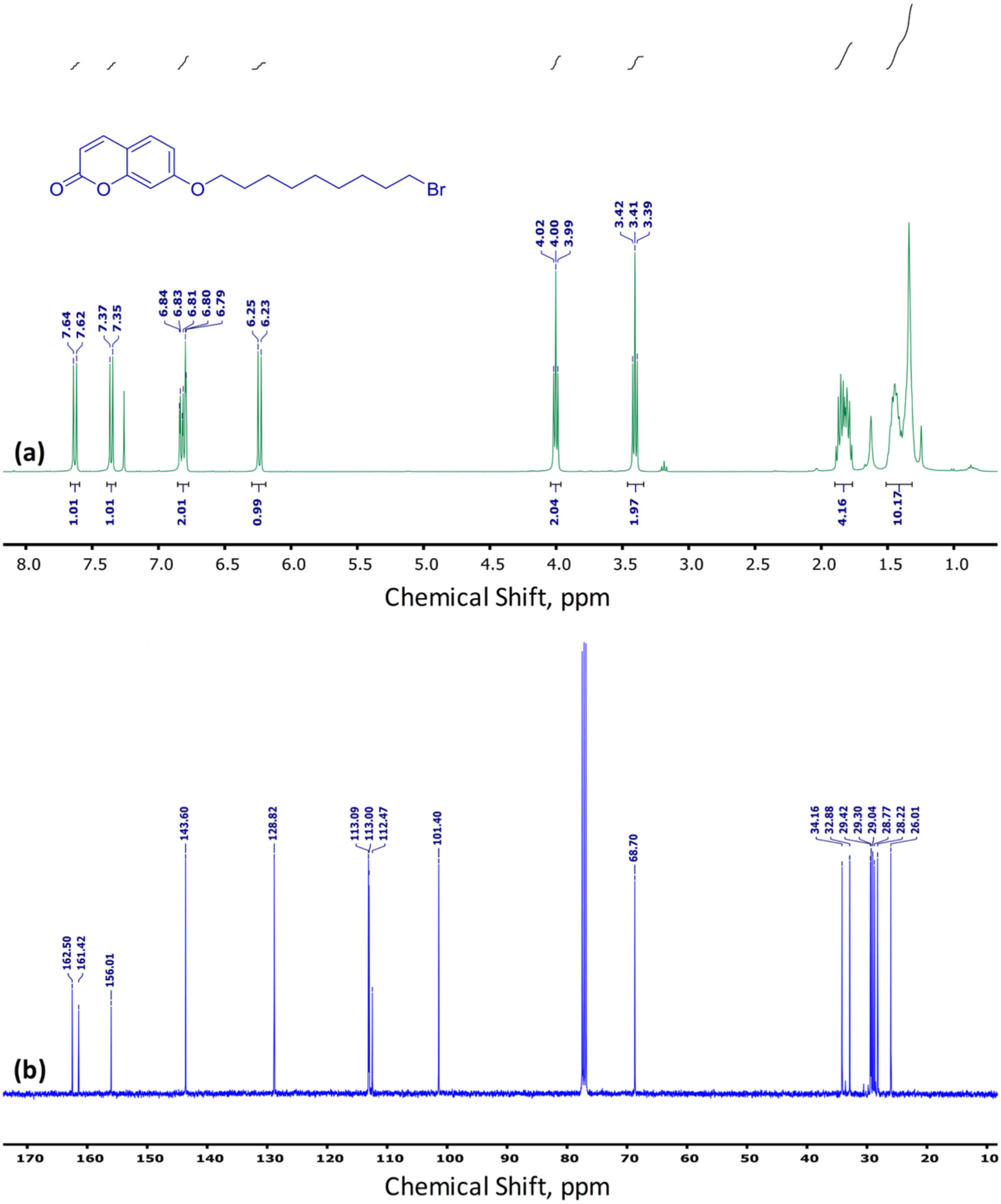

Figure S1. (a) ^{1}H ($CDCl_3$, 400 MHz) and (b) ^{13}C ($CDCl_3$, 100 MHz) NMR spectra of **M1**.

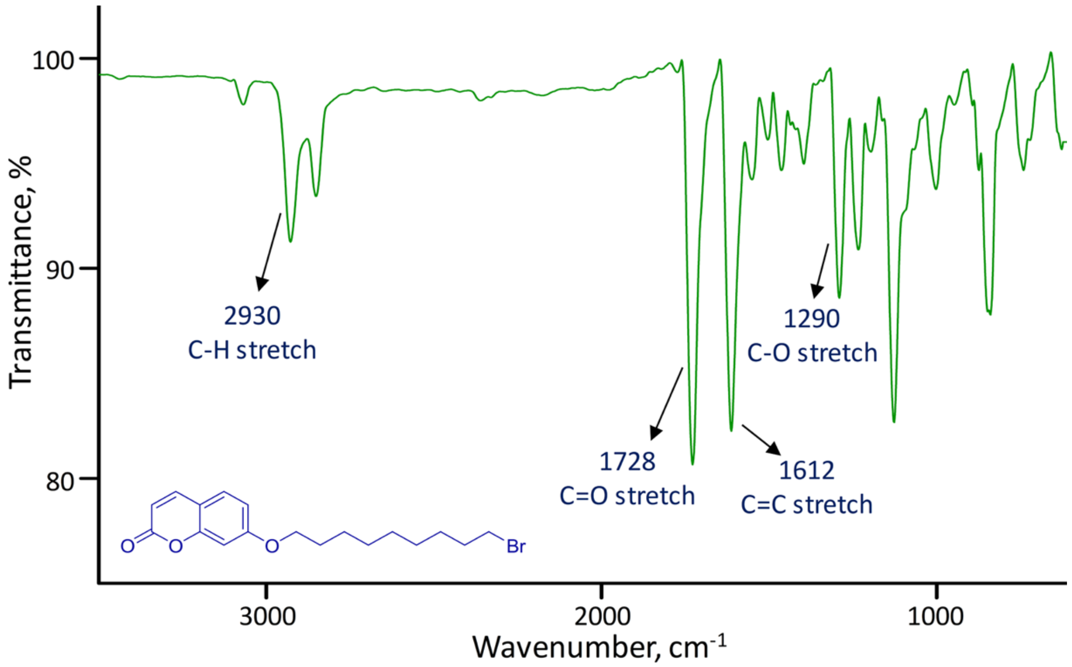

Figure S2. FT-IR spectrum of **M1**.

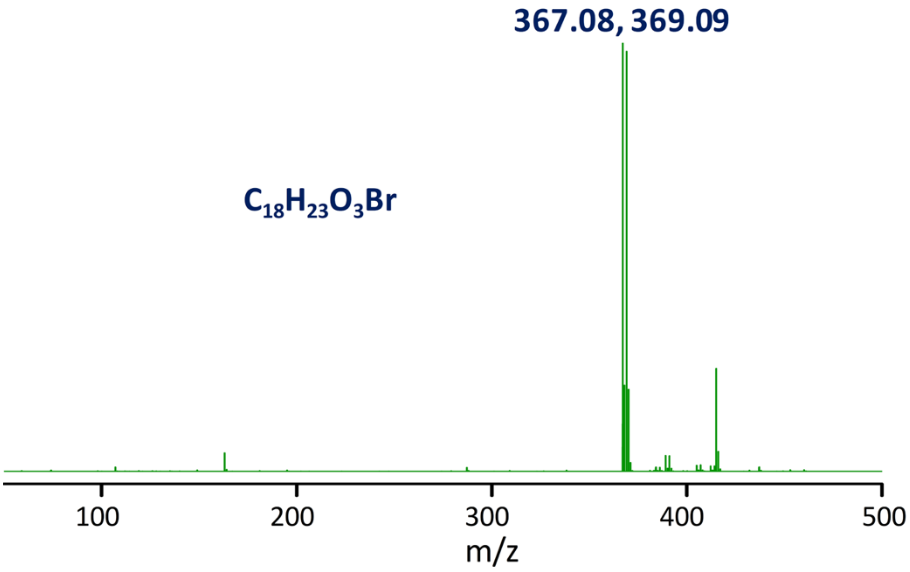

Figure S3. HR-MS of **M1**.

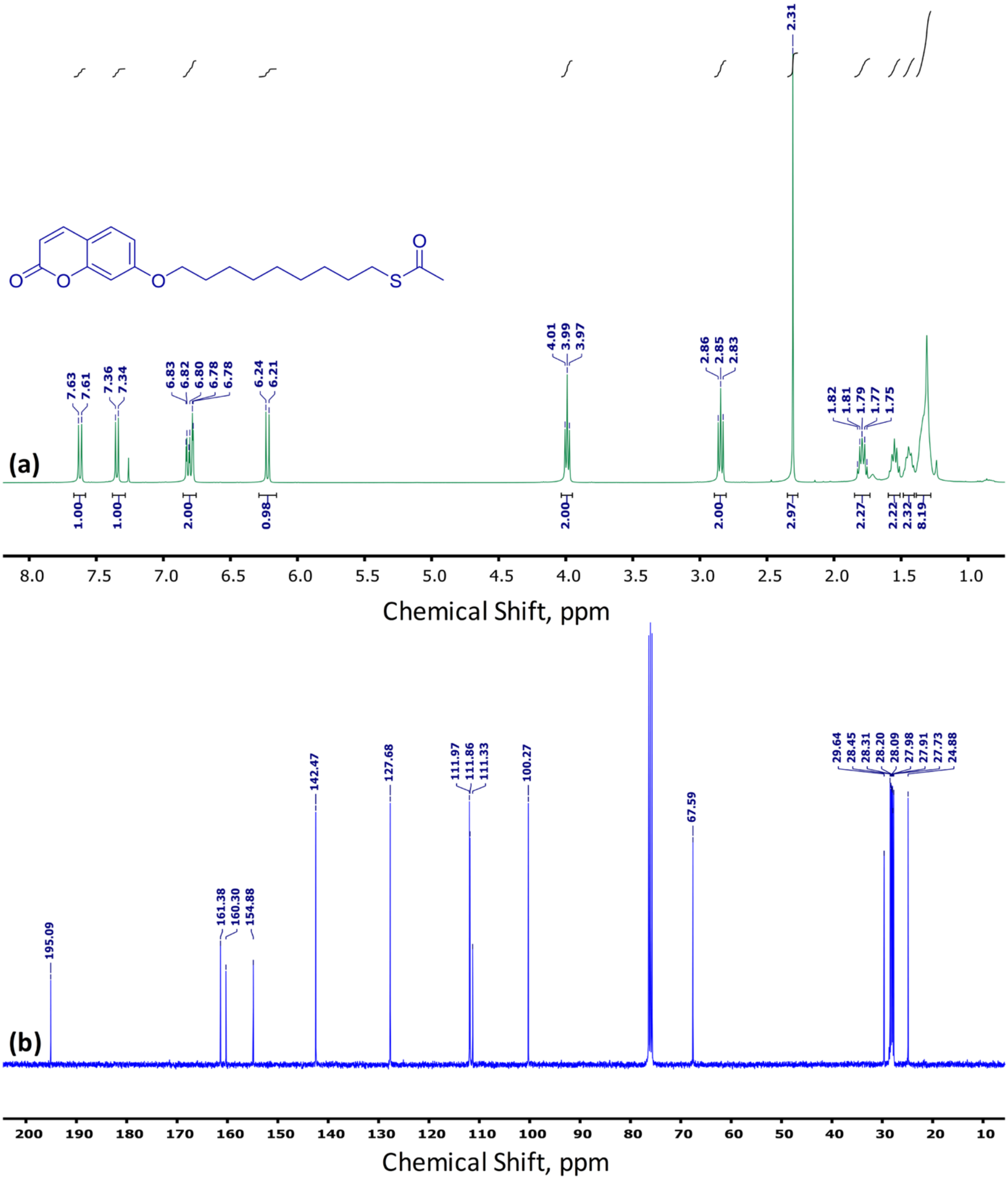

Figure S4. (a) ^{1}H ($CDCl_3$, 400 MHz), (b) ^{13}C ($CDCl_3$, 100 MHz) NMR spectra of **M2**.

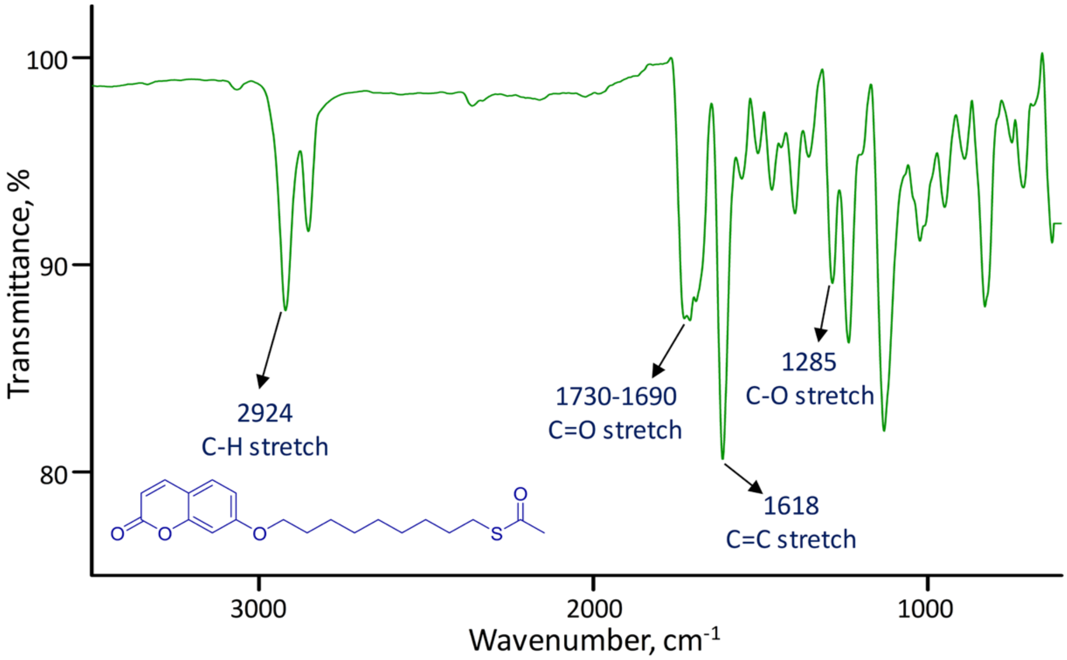

Figure S5. FT-IR spectrum of **M2**.

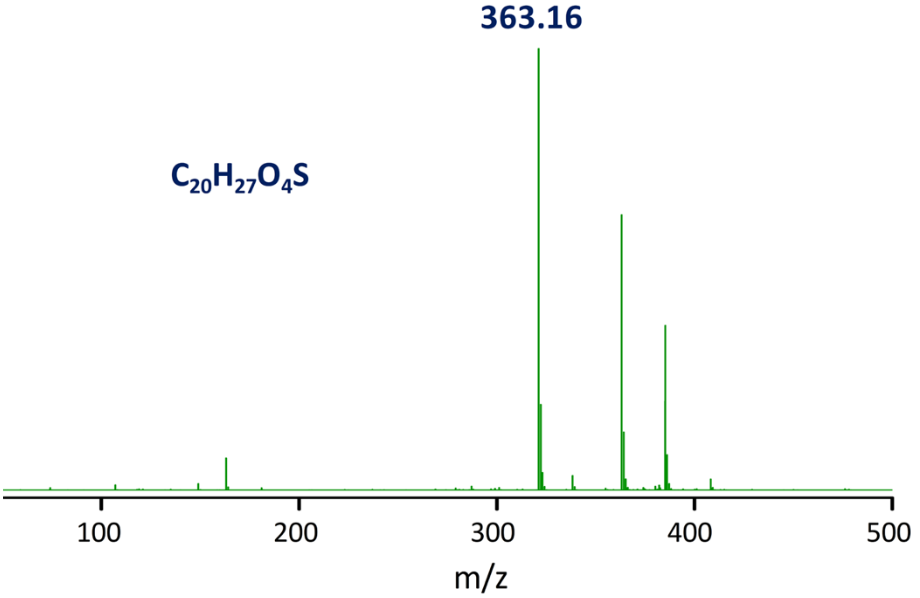

Figure S6. HR-MS of **M2**.

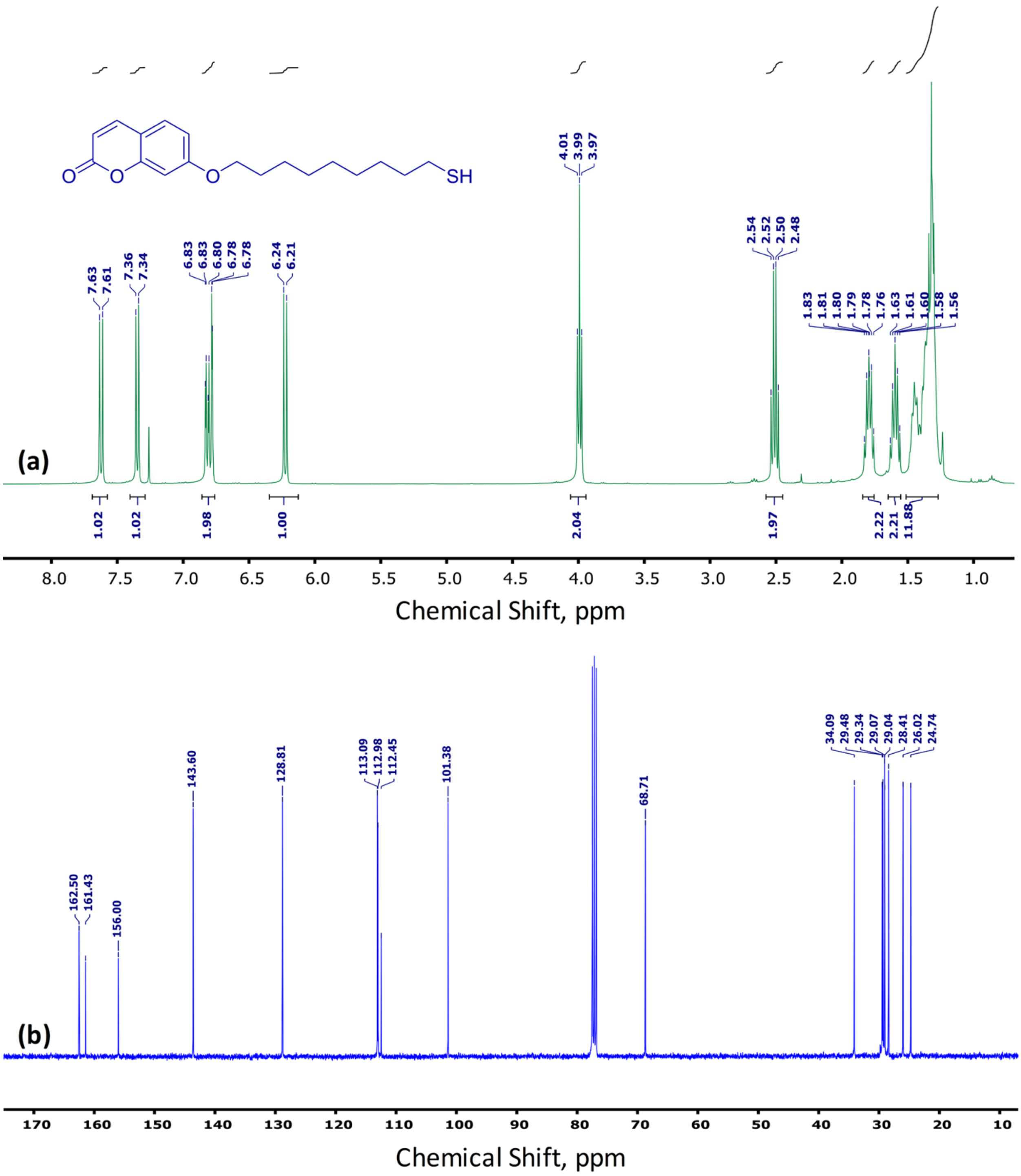

Figure S7. (a) ^{1}H ($CDCl_3$, 400 MHz), (b) ^{13}C ($CDCl_3$, 100 MHz) NMR spectra of **M3**.

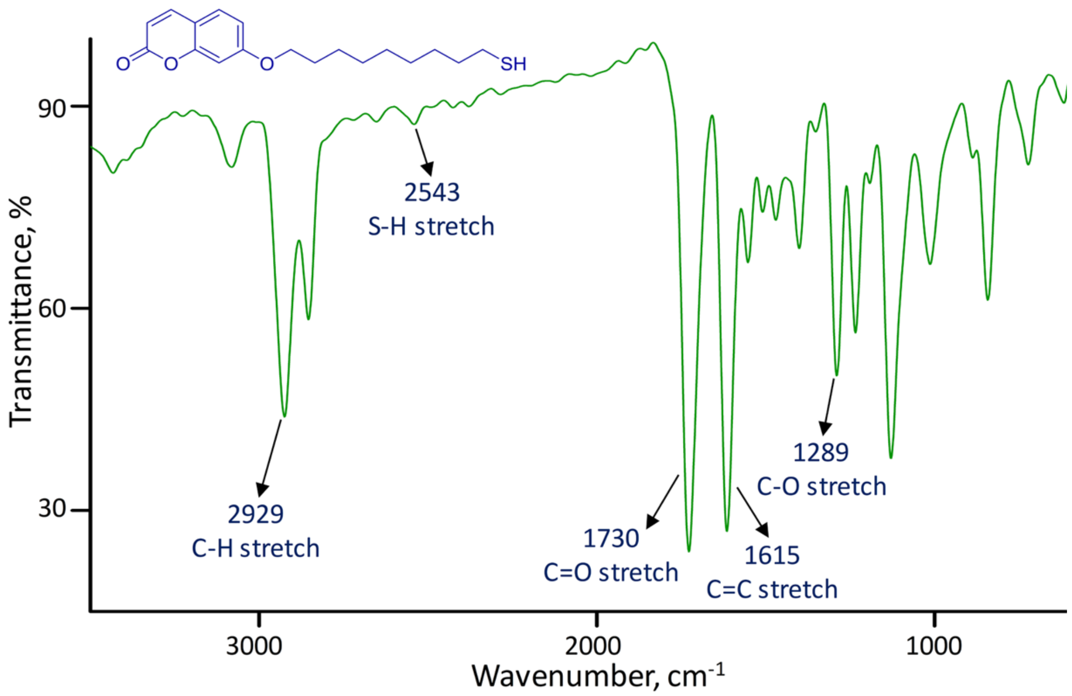

Figure S8. FT-IR spectrum of **M3**.

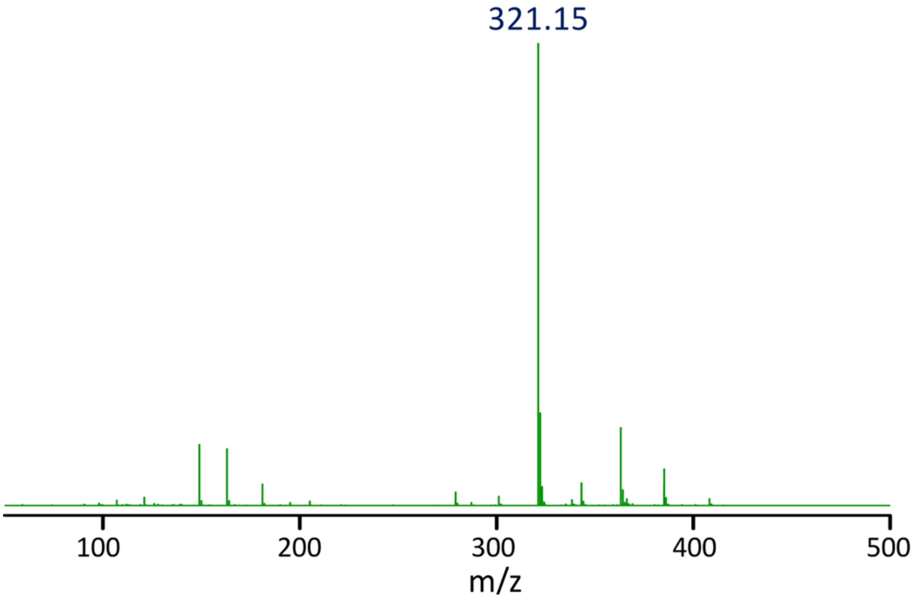

Figure S9. HR-MS of **M3**.

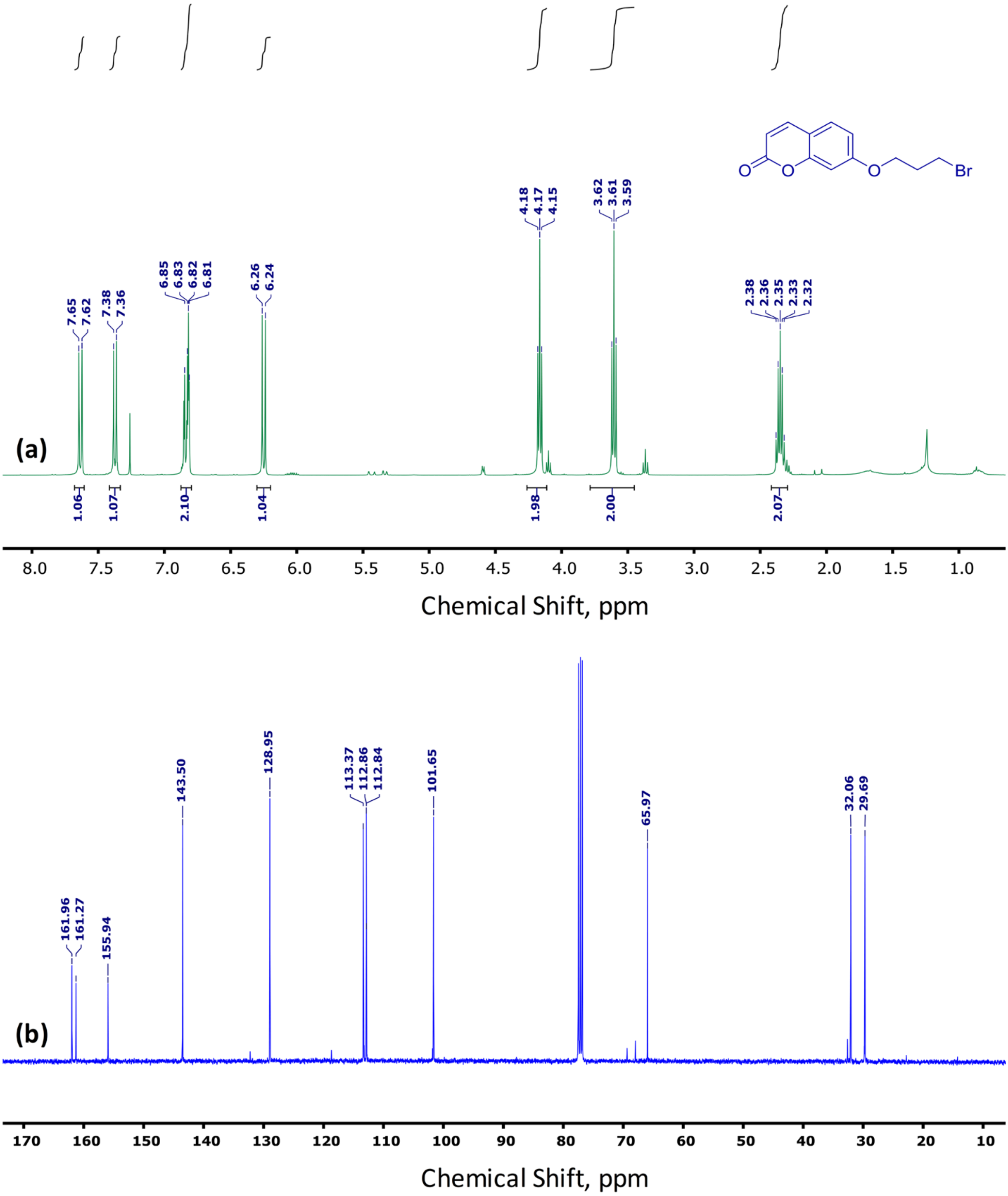

Figure S10. (a) ^{1}H (CDCl$_3$, 400 MHz), (b) ^{13}C (CDCl$_3$, 100 MHz) NMR spectra of **M4**.

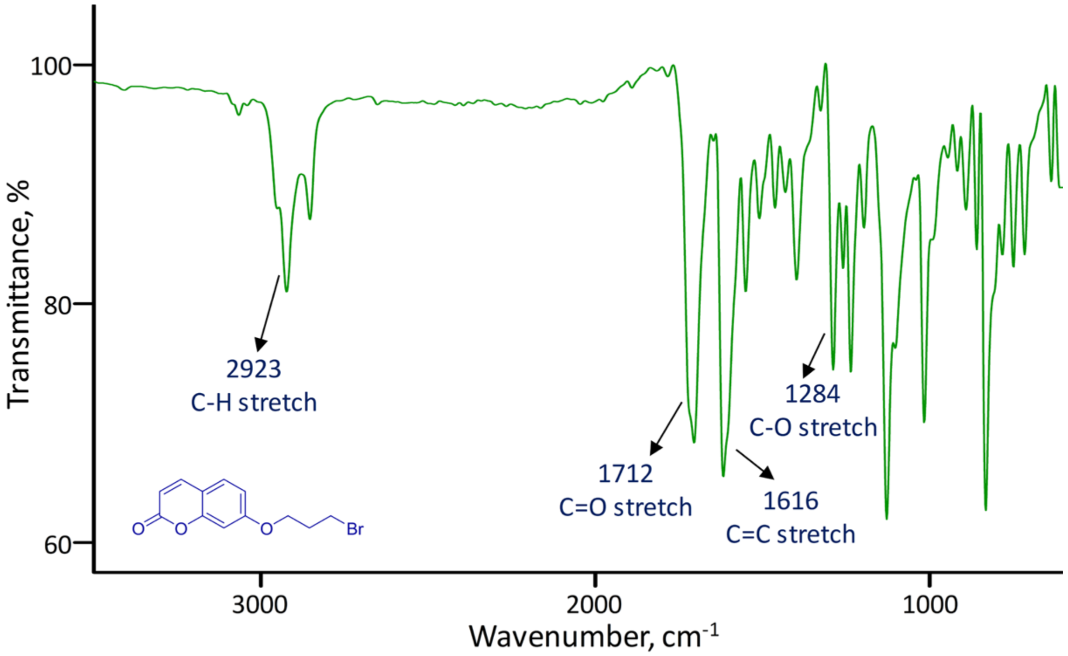

Figure S11. FT-IR spectrum of **M4**.

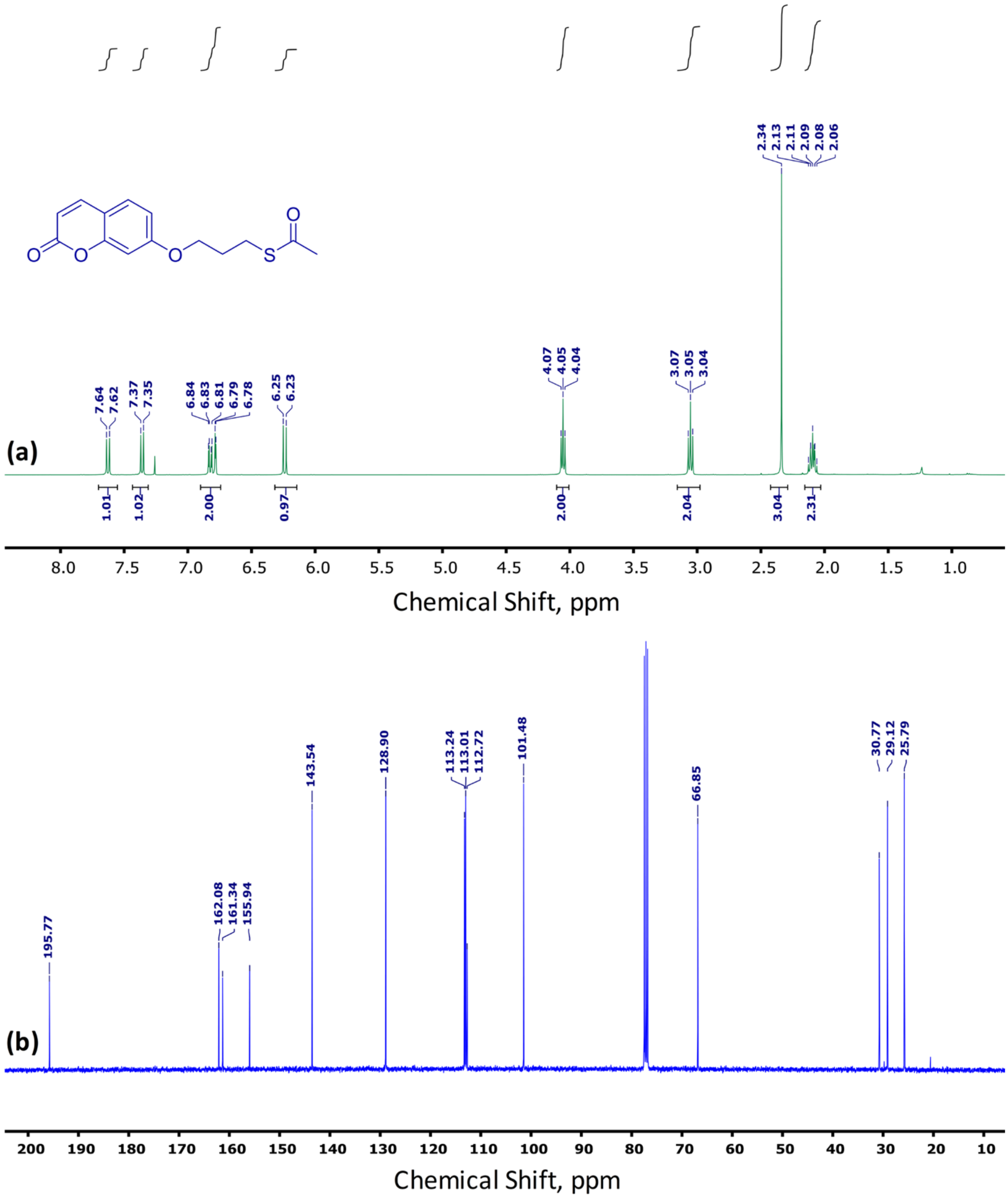

Figure S12. (a) ^{1}H ($CDCl_3$, 400 MHz), (b) ^{13}C ($CDCl_3$, 100 MHz) NMR spectra of **M5**.

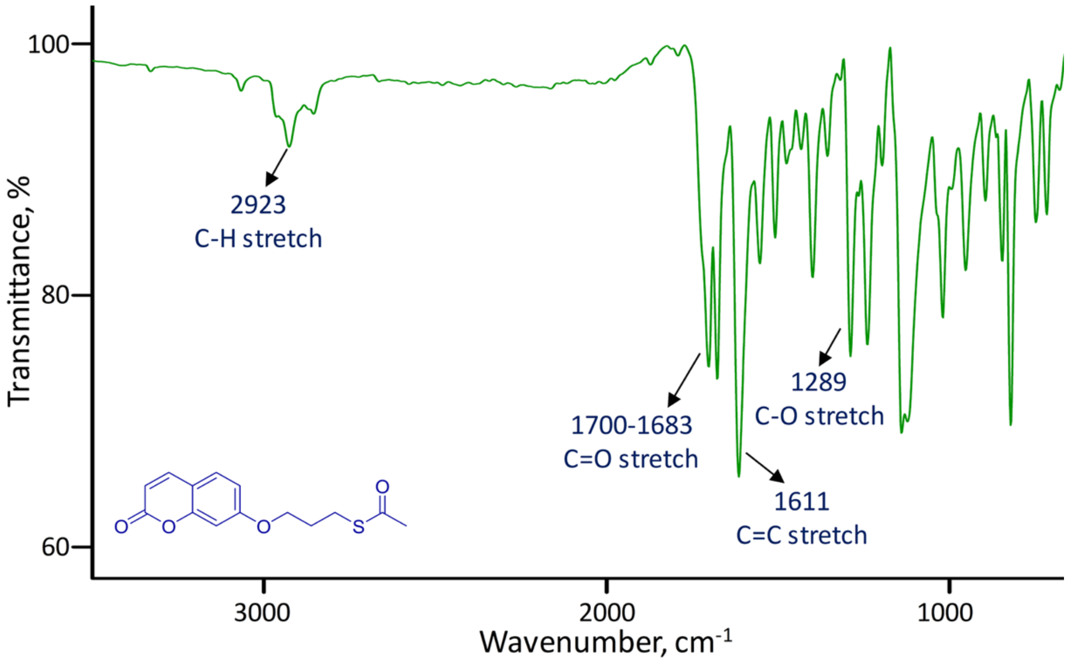

Figure S13. FT-IR spectrum of **M5**.

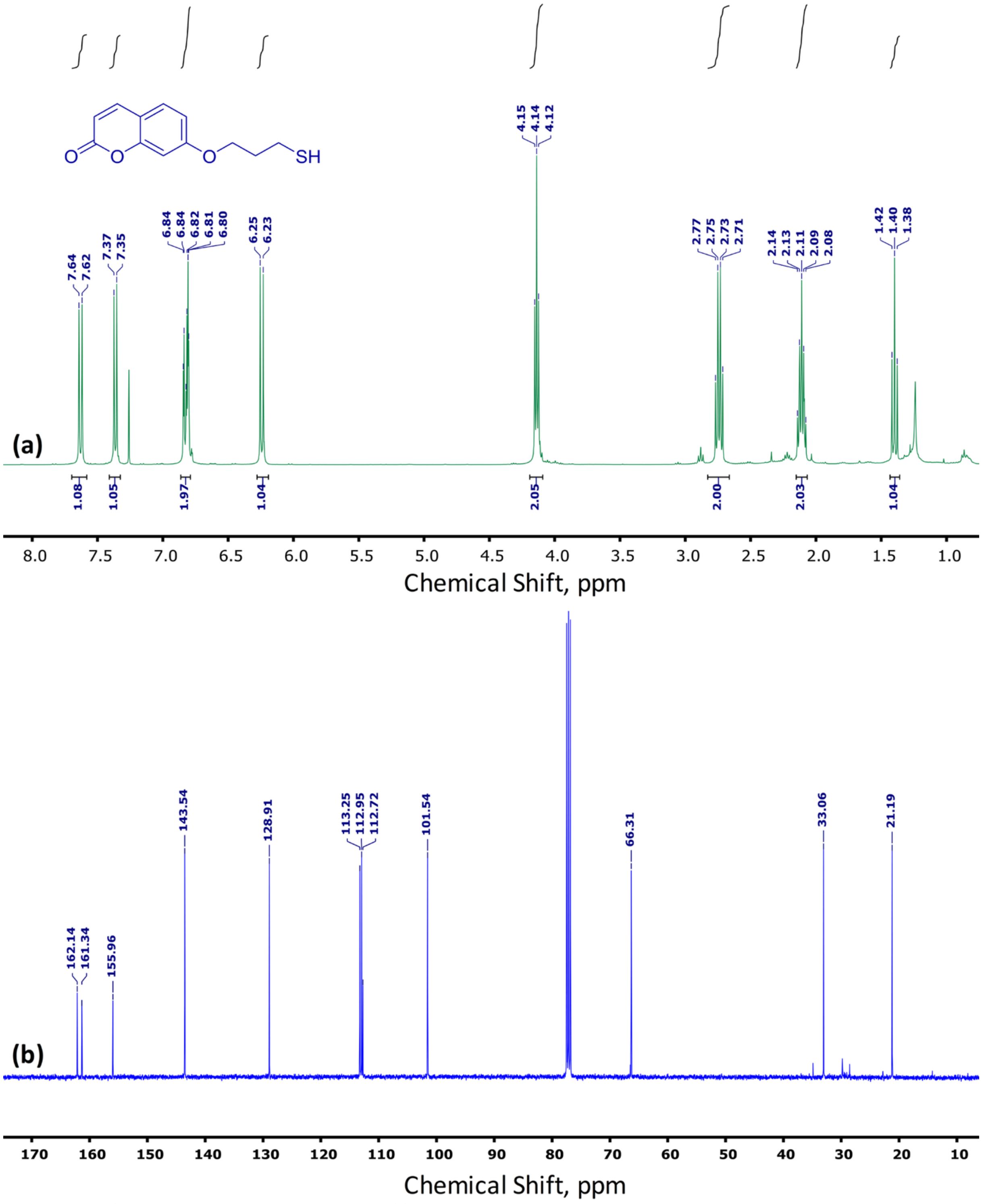

Figure S14. (a) ^{1}H ($CDCl_3$, 400 MHz), (b) ^{13}C ($CDCl_3$, 100 MHz) NMR spectra of **M6**.

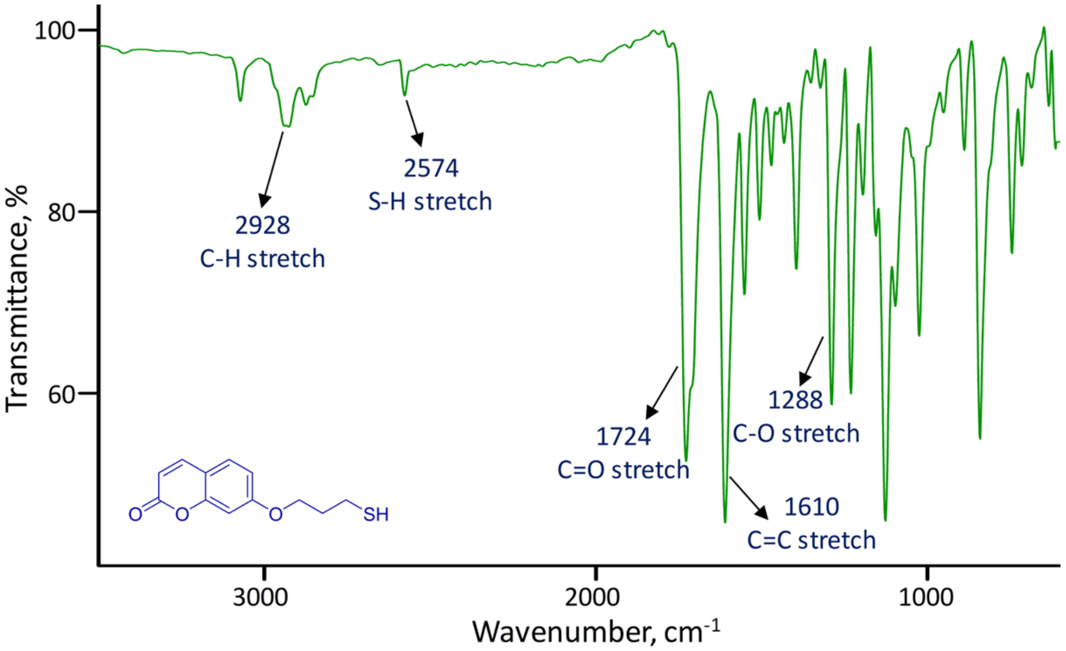

Figure S15. FT-IR spectrum of **M6**.

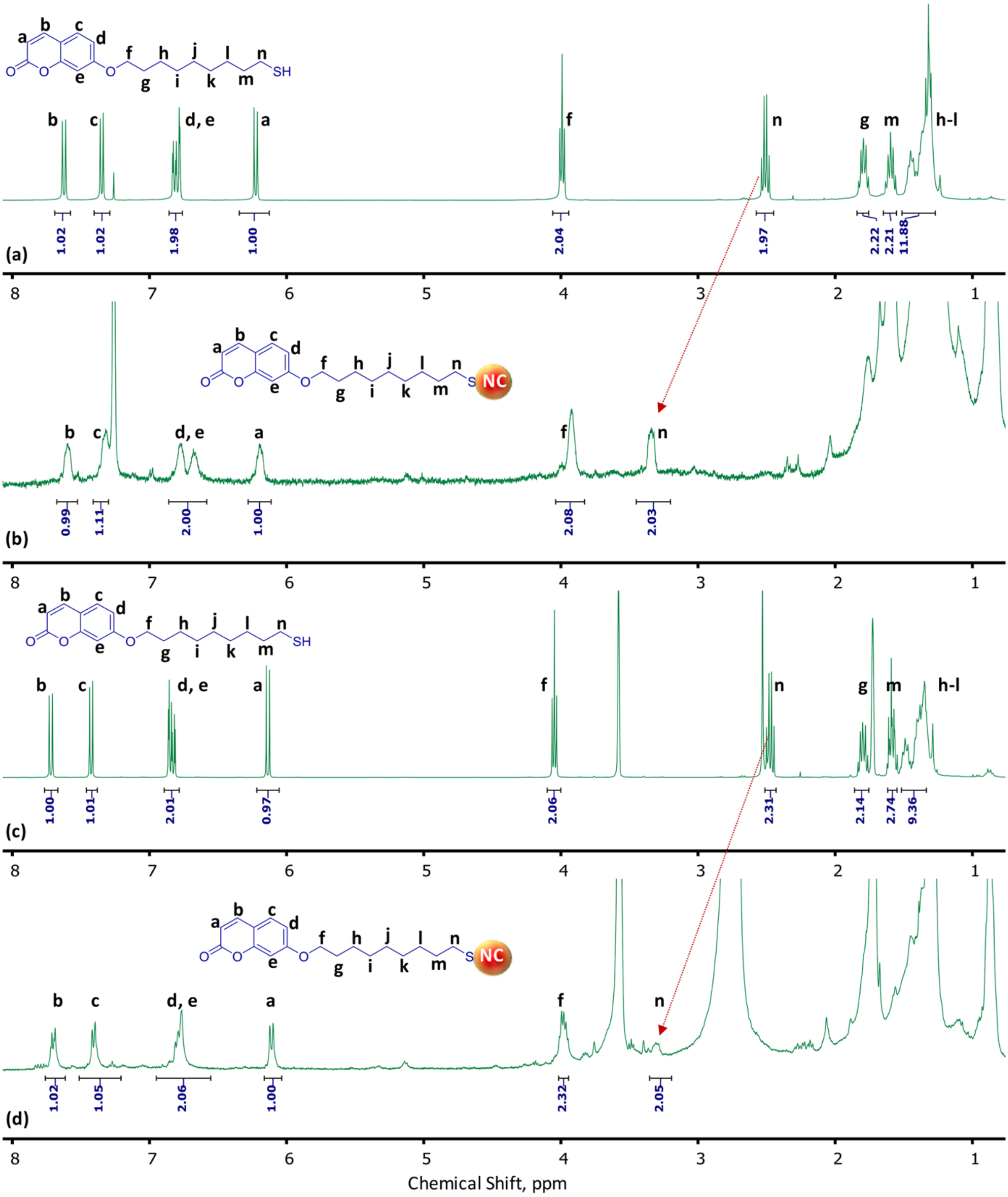

Figure S16. ^{1}H NMR (400 MHz) spectra of (a and c) C$_9$-CMT and (b and d) [Au$_{25}$(C$_9$-CMT)$_{18}$]$^-$ NCs in (a and b) in CDCl$_3$ and (c and d) in THF-d$_8$.

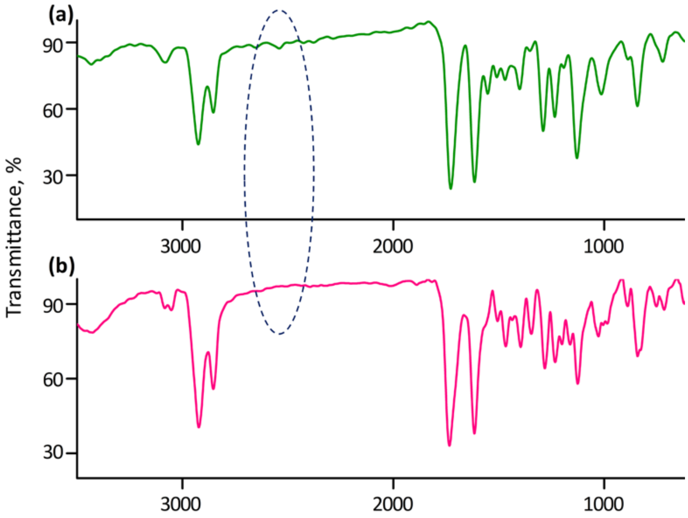

Figure S17. FT-IR spectra of (a) C9-CMT and (b) $[Au_{25}(C_9\text{-}CMT)_{18}]^-$ NCs.

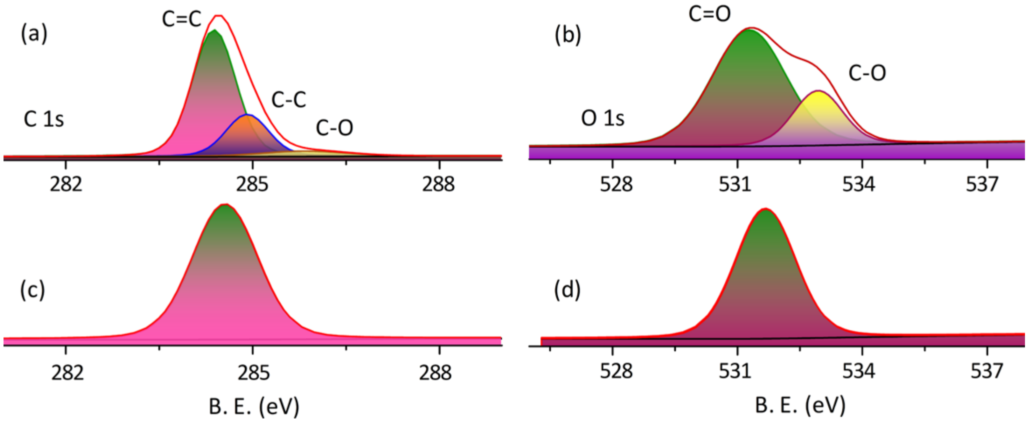

Figure S18. XPS spectra recorded from (a and b) $[Au_{25}(C_9\text{-}CMT)_{18}]^-$ and (c and d) $[Au_{25}(PET)_{18}]^-$ NCs show the presence of (a and c) C1s and (b and d) O1s.

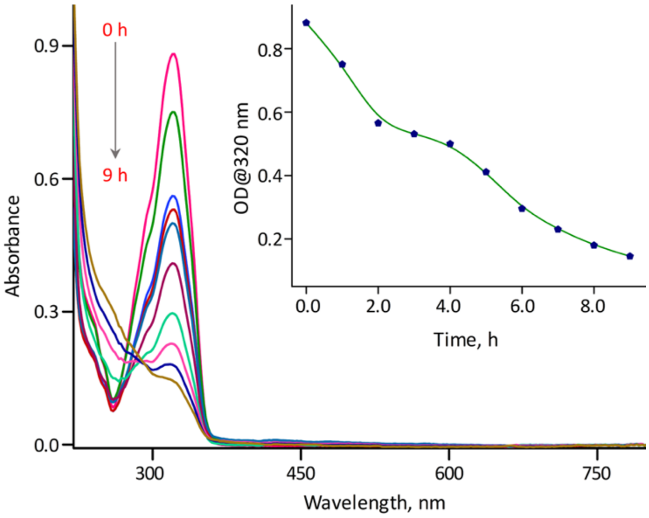

Figure S19. Temporal UV-Vis absorption spectra of C9-CMT in THF under 365 nm illumination. The changes in OD as a function of illumination time are shown in the inset.

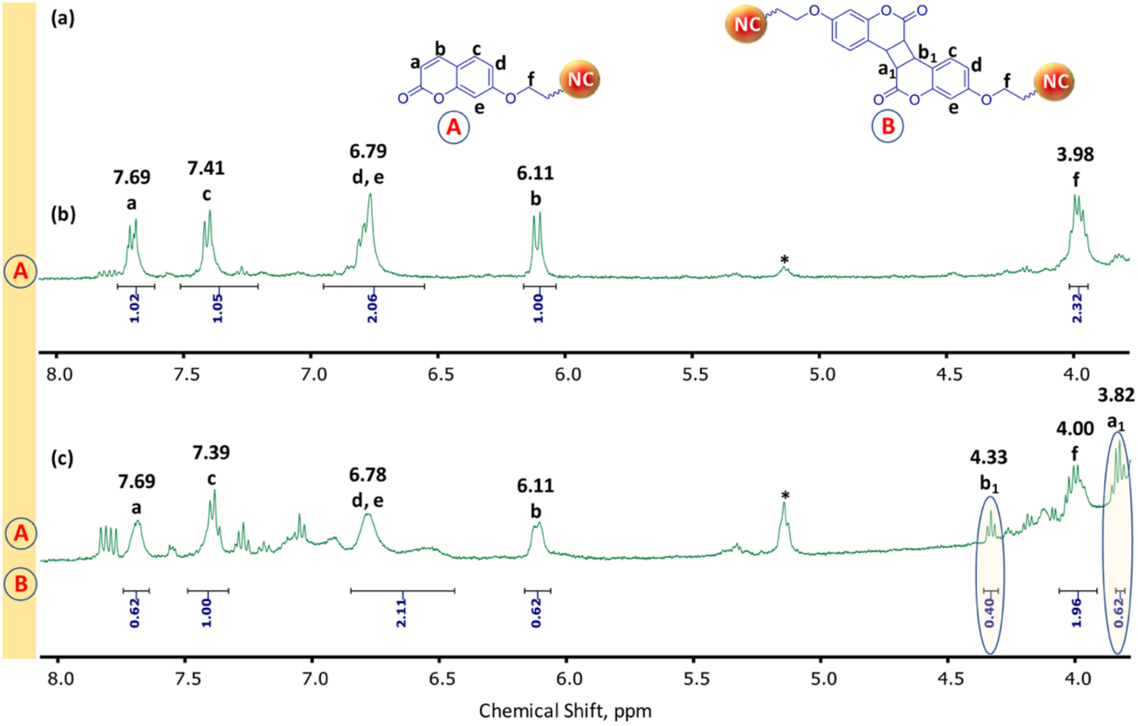

Figure S20. ^{1}H NMR (400 MHz, THF-d_8) spectra recorded from (b) NC and (c) toroidal assembly. Two different possible combinations are shown in scheme (a). The cyclobutane protons are marked. *Represents the unassigned peak.

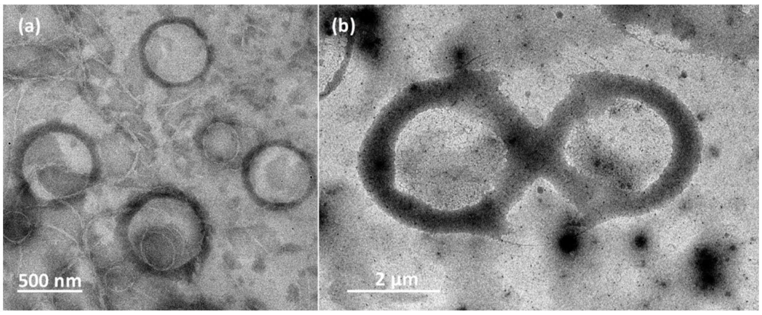

Figure S21. TEM micrographs captured from the NC solution assembled under high power light source.

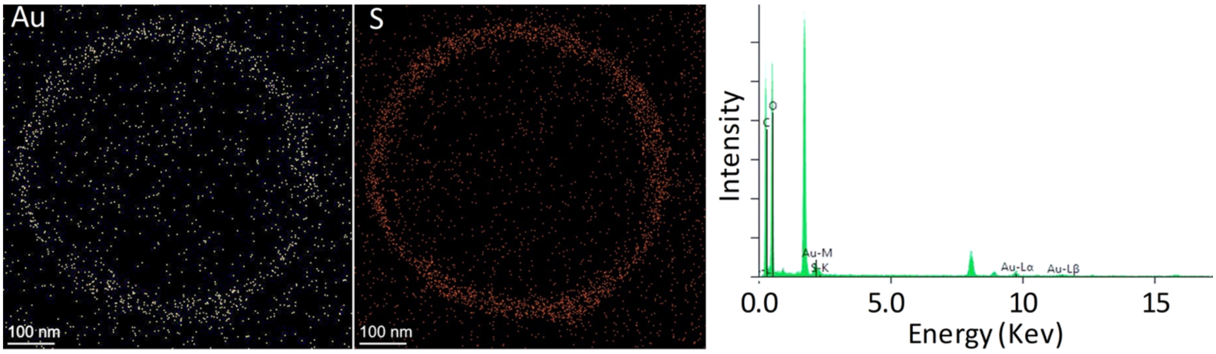

Figure S22. Elemental maps (gold and sulfur) and corresponding spectrum recorded from a single toroid.

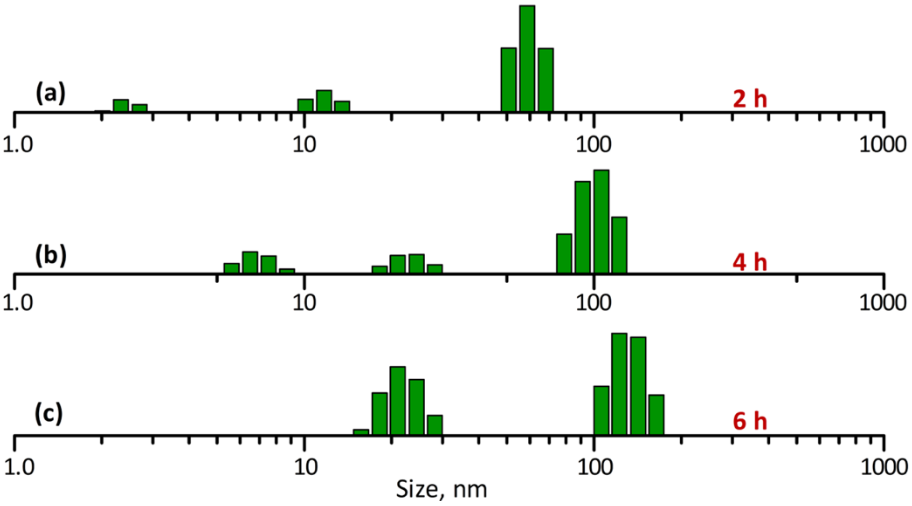

Figure S23. DLS spectra recorded during the solution state assembly of NCs.

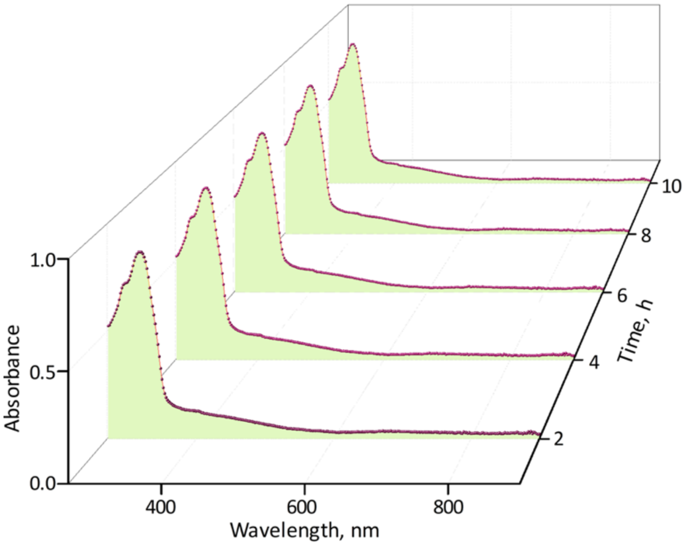

Figure S24. The temporal UV-Vis absorption spectra recorded from toroidal solution under dark.

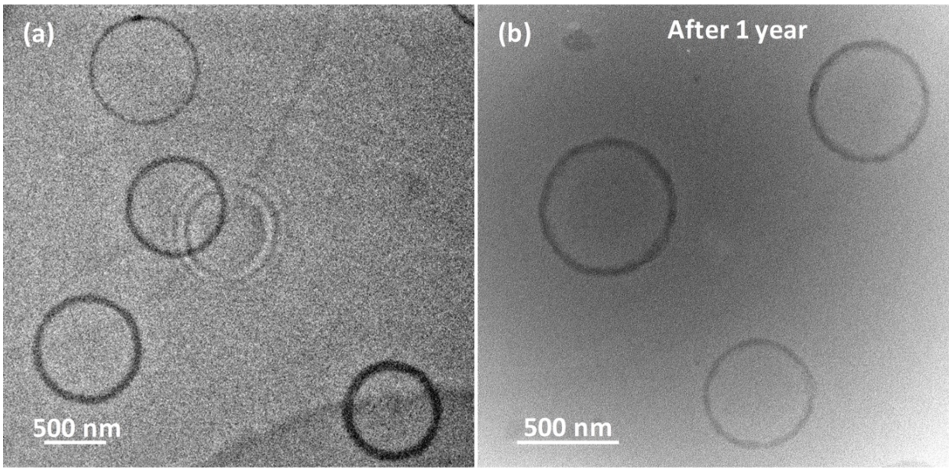

Figure S25. TEM micrographs of toroids recorded (a) before and (b) after 1 year.

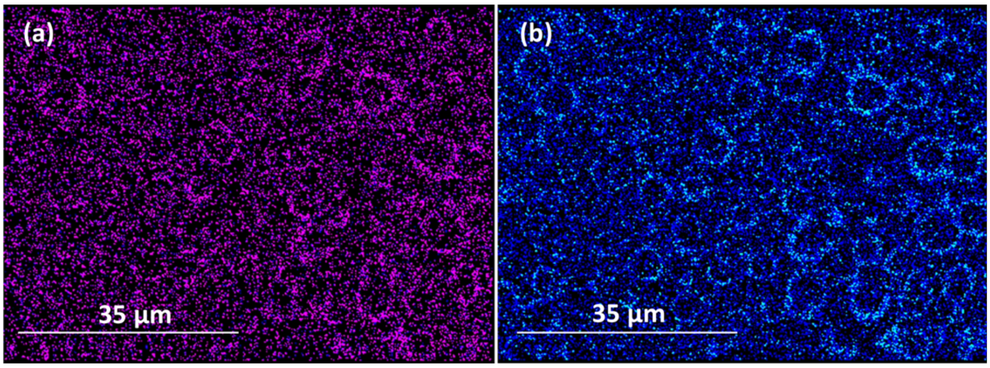

Figure S26. Large area elemental maps recorded from toroids show the presence of (a) gold and (b) sulfur.

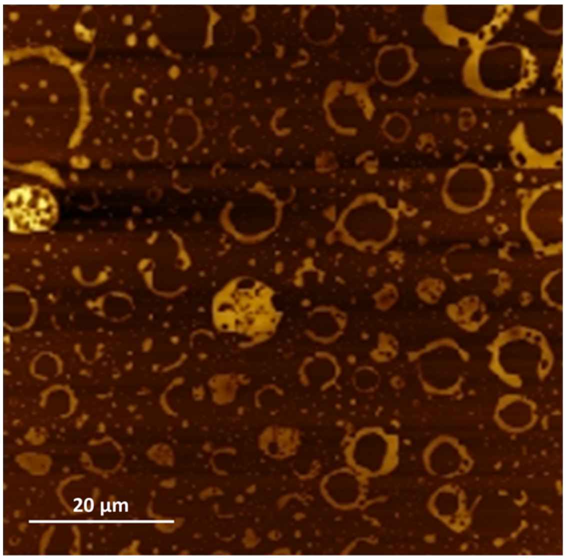

Figure S27. Large area AFM image of toroids.

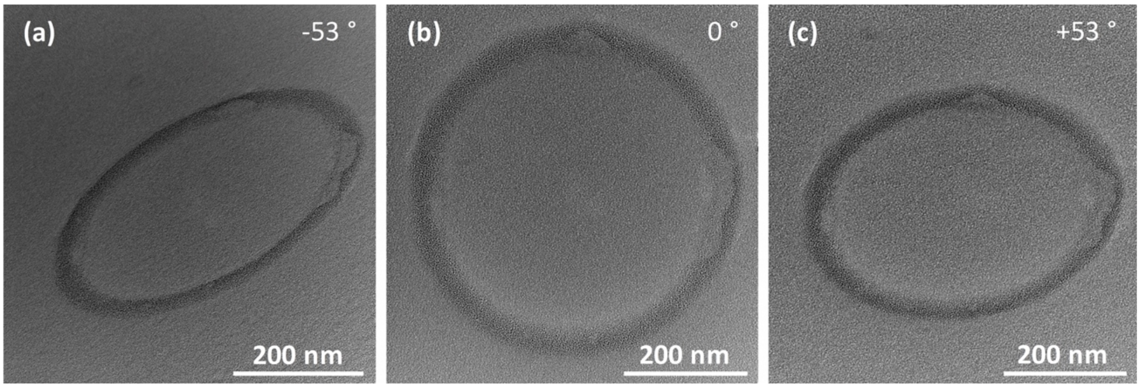

Figure S28. TEM images of a single toroid at different tilt angles.

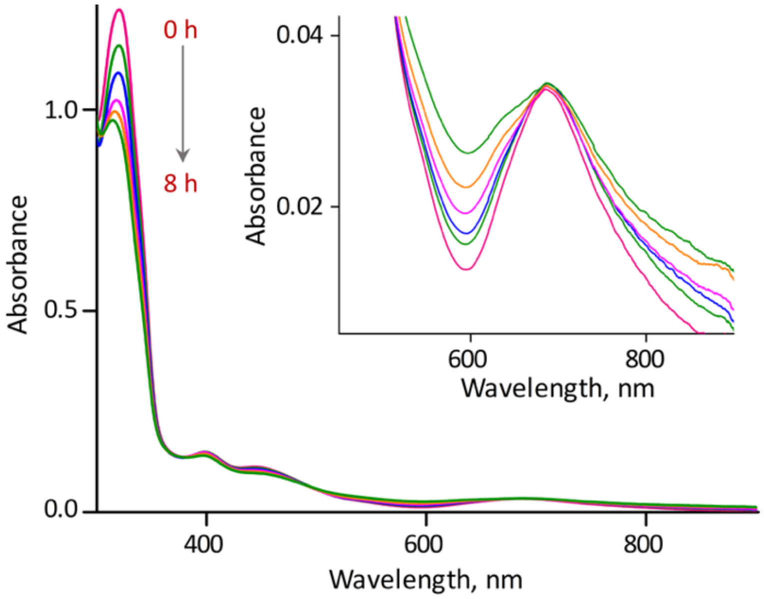

Figure S29. The temporal UV-Vis absorption spectra recorded from $[Au_{25}(C_9\text{-}CMT)_{18}]^-$ NCs in the presence of 5-FU under 365 nm illumination. The inset shows an enlarged view of the HOMO-LUMO band of NC.

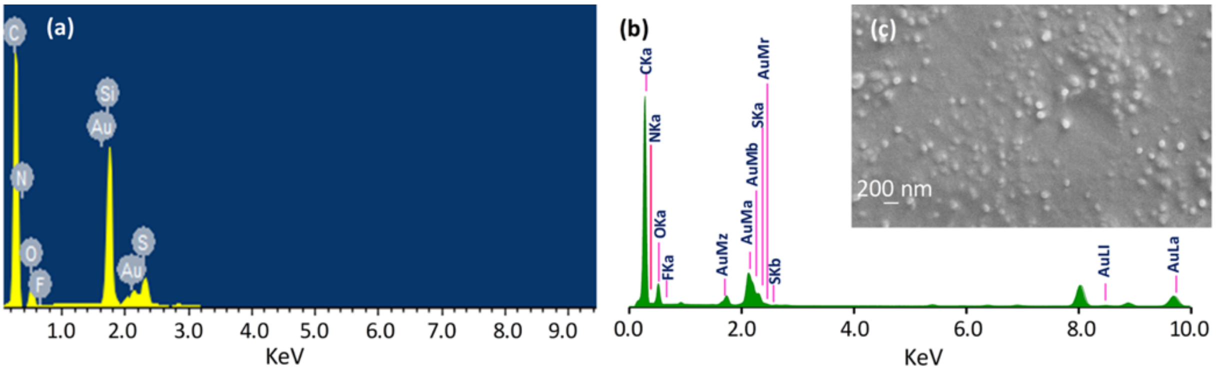

Figure S30. (a) FESEM and (b) STEM EDS spectrum recorded from NC-FU spherical assembly. (c) FESEM micrograph of NC-FU assembly.

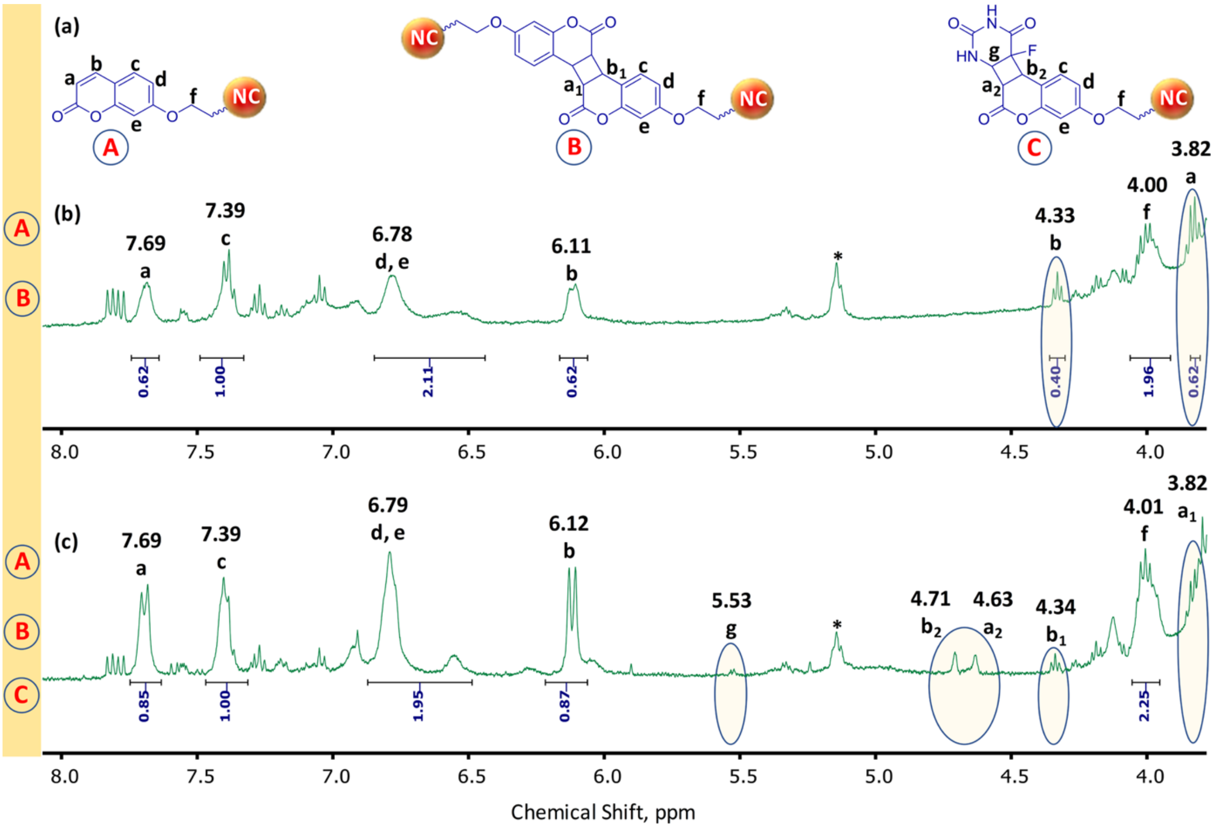

Figure S31. ^{1}H NMR (400 MHz. THF-d_8) spectra recorded from (b) toroidal assembly and (c) NC-FU conjugate. Three different possible combinations are shown in scheme (a). The cyclobutane protons are marked. *Represents the unassigned peak.

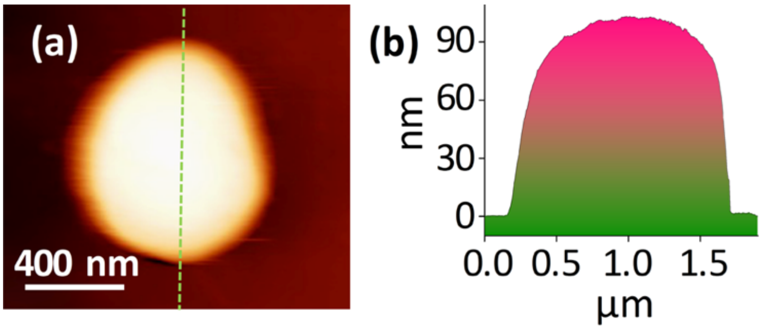

Figure S32. (a) AFM topography and (b) height profile of a single NC-FU assembled sphere.

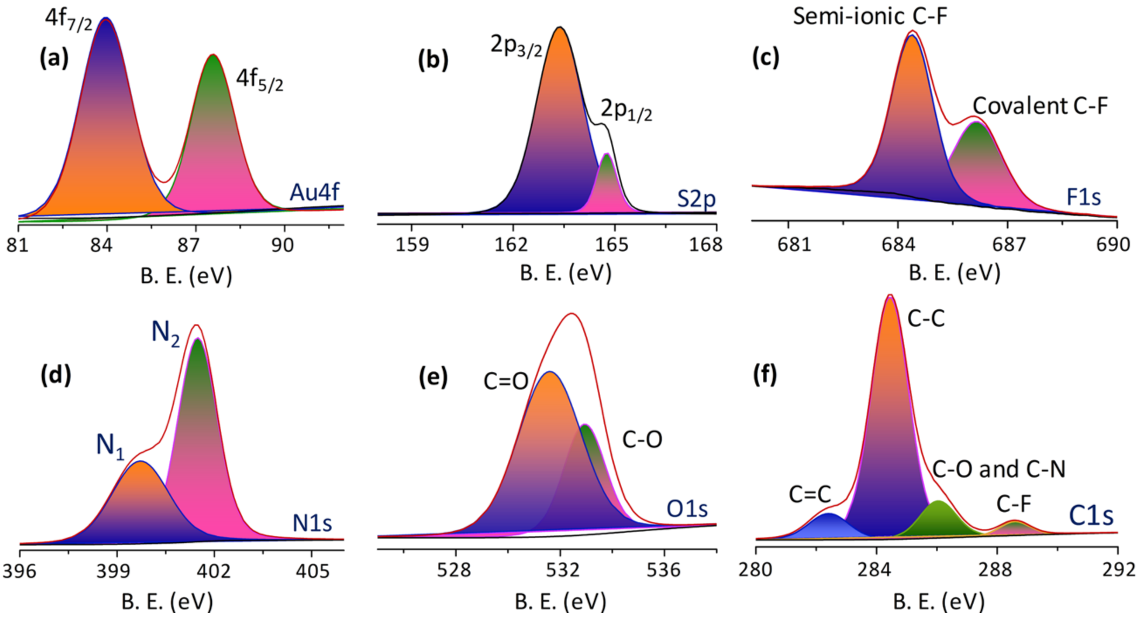

Figure S33. The XPS spectra recorded from the NC-FU assembly show the presence of (a) Au 4f, (b) S 2p, (c) F1s, (d) N1s, (e) O1s, and (f) C1s.

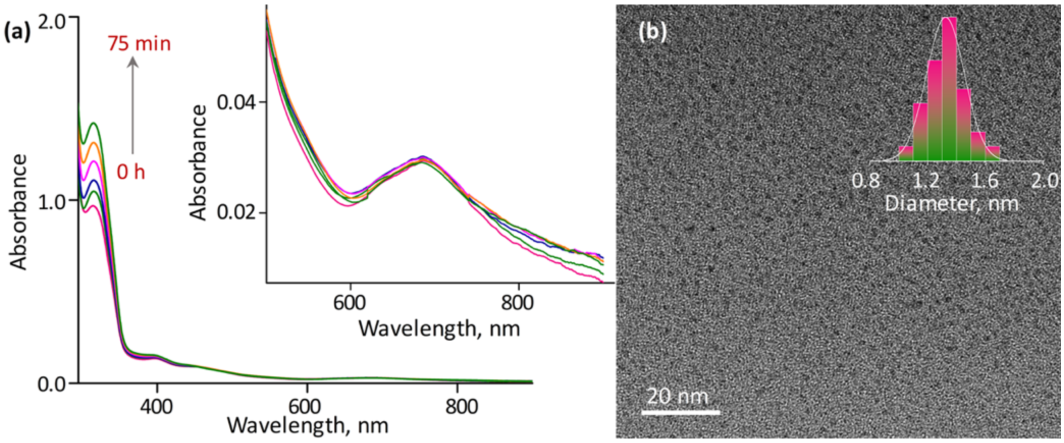

Figure S34. (a) Temporal UV-Vis absorption spectra recorded from NC-FU conjugate solution during the unloading of the drug under 254 nm illumination. An expanded view of the HOMO-LUMO band is shown in the inset. (b) TEM micrograph captured after the completion of drug unloading shows the presence of individual NCs.

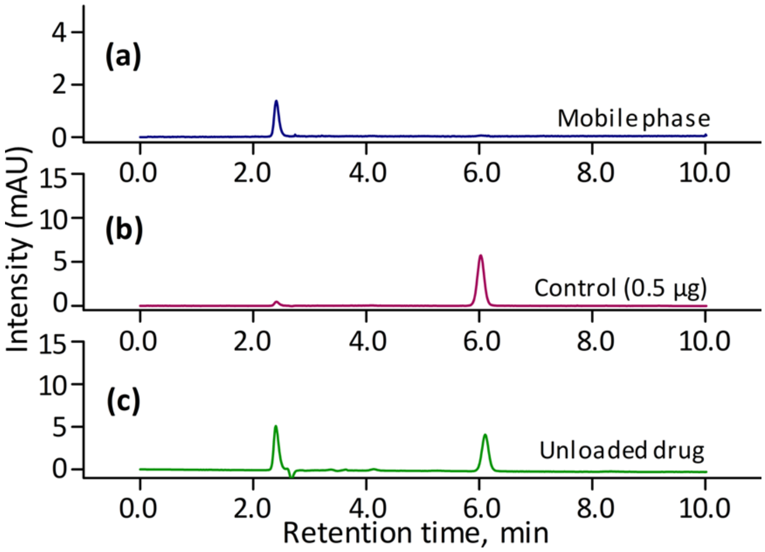

Figure S35. HPLC chromatogram shows the separation and retention time of (a) the mobile phase, (b) the control drug, and (c) the unloaded drug from the NC surface after 254 nm illumination.

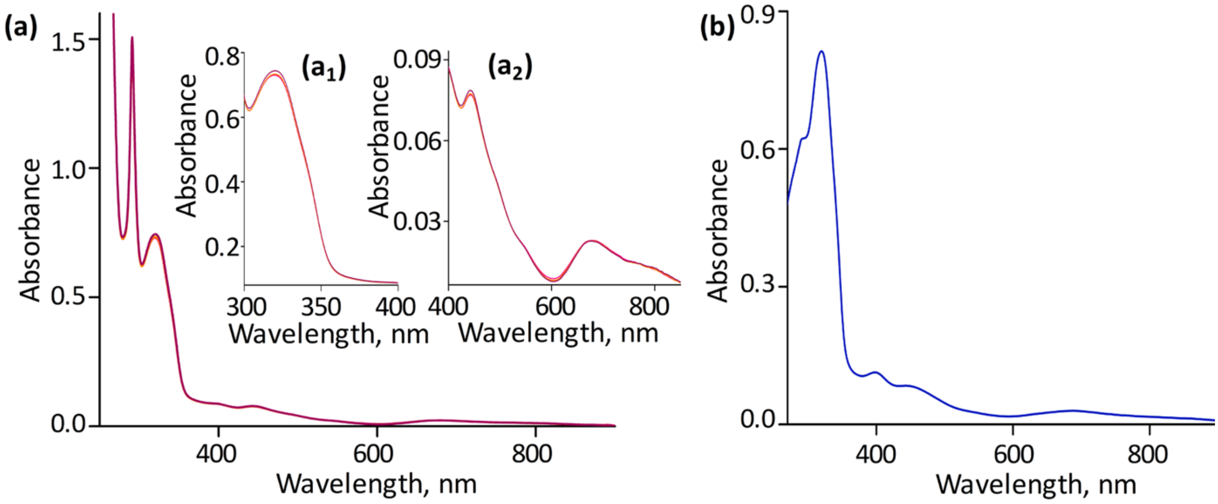

Figure S36. (a) Temporal UV-Vis absorption spectra recorded from a mixture of NC and 5-FU under the dark. Insets a_1 and a_2 show the expanded view of the optical absorption features of (a_1) coumarin and (a_2) NCs. (b) The UV-Vis absorption spectrum of NC after precipitation and washing process.